



Temperature gradients and evaluation of thermoelastic properties in the synchrotron-based laser-heated diamond cell

Abby Kavner^{a,*}, Wendy R. Panero^b

^a Earth and Space Science Department, Institute of Geophysics and Planetary Physics, UCLA, Los Angeles, CA 90095-1567, USA

^b Department of Geological Sciences, University of Michigan, Ann Arbor, MI 48109, USA

Received 30 November 2002; received in revised form 3 December 2003; accepted 6 December 2003

Abstract

Reliable determinations of thermoelastic properties inside the laser-heated diamond cell depend critically on accurate measurement of temperature, temperature gradients, and the relationship between the hotspot and the X-ray beam. Here we examine these issues and their relative importance in interpreting data from synchrotron-based studies of materials at high pressures and temperatures. When combining laser heating and X-ray diffraction, temperature gradients must be measured and compared with the size of the X-ray beam in synchrotron-based laser-heated diamond anvil cell experiments in order to avoid systematically overestimating the actual average temperature of the X-rayed volume. For a laser-heated sample with a hotspot that drops to 75% of its value at the edge of the X-ray beam, the temperature measured at the hotspot center overestimates the actual average temperature by 17%, leading to up to a 20% underestimate of thermal expansion. As temperature gradients become steeper with increasing pressure, the temperature measured at the hotspot center increasingly overestimates the average temperature of the X-rayed volume, which further distorts measurements of higher order thermoelastic parameters. This can help to explain a wide variety of anomalous experimental results, including low thermal expansion values, and a higher than expected decrease of thermal expansion with increasing pressure without necessarily calling upon constant volume conditions in the cell. To help address these issues, we present four semi-independent methods to calculate temperature gradients inside the laser-heated diamond cell by taking advantage of the Planck's law relationships between spectral intensity, integrated intensity, and temperature. Together, these methods yield a precise determination of the radial temperature gradient and provide an internal consistency check on the accuracy of the absolute temperature measurement. We show how these methods can be used to recover precise measurements of temperature gradients even in the presence of optical chromatic aberrations. © 2004 Elsevier B.V. All rights reserved.

Keywords: Laser heating; Spectroradiometry; Chromatic aberration; Diamond anvil cell; Thermoelastic properties; Temperature measurement

1. Introduction

To model and predict planetary structure and dynamics, and to properly interpret results from seismic

data, we require accurate and precise measurements of the behavior of minerals at the high pressures and temperatures relevant to planetary interiors. The laser-heated diamond anvil cell is a powerful experimental tool to measure material properties in situ, including pressure–volume–temperature (P – V – T) equations of state (Fiquet et al., 1998; Dewaele et al., 2000; Shim et al., 2000), phase boundaries (Boehler et al., 1990; Saxena et al., 1994; Kavner

* Corresponding author. Tel.: +1-310-206-3675;

fax: +1-310-825-2779.

E-mail addresses: akavner@ucla.edu, akavner@igpp.ucla.edu, akavner@ess.ucla.edu (A. Kavner).

et al., 2001; Shim et al., 2001), melting curves (Williams and Jeanloz, 1990; Williams et al., 1991; Boehler, 1992; Lazor et al., 1993; Sweeney and Heinz, 1993; Yoo et al., 1993; Boehler and Ross, 1997; Boehler et al., 1997; Kavner and Jeanloz, 1998a,b; Shen et al., 1998; Sitaud and Thevenin, 1999) and transport properties (Andrault, 2001). Because temperature plays a tremendous role in governing the physical behavior of materials, the ability to interpret data obtained in the laser-heated diamond cell hinges upon a critical and quantitative evaluation of both precision and accuracy of the temperature measurement.

Synchrotron-based experiments designed to simultaneously measure crystal structure and volume inside the diamond cell are especially sensitive to the presence of temperature gradients which are present under most laser-heating conditions (Boehler et al., 1990; Williams et al., 1991; Boehler and Chopelas, 1991; Jeanloz and Kavner, 1996; Kavner et al., 1998; Andrault and Fiquet, 2001; Shen et al., 2001; Yagi et al., 2001; Panero and Jeanloz, 2001a). The desire for uniform temperatures in an experiment designed to measure equilibrium thermodynamic properties has generated a significant experimental effort to minimize temperature gradients across the width of the X-ray beam and thickness of the sample. These efforts, including heating with a high-powered CO₂ laser (Boehler and Chopelas, 1991) combining external resistance heating and laser heating (Li et al., 1996), heating both sides of the sample simultaneously using double-hot-plate heating (Shen et al., 2001), mixing the TEM₀₁ and TEM₀₀ laser modes (Shen et al., 2001), and increasing the gasket thickness (Boehler et al., 1997; Panero and Jeanloz, 2001b) have yielded mixed success.

Partially as a response to technical difficulties in measuring temperatures across intensity gradients, and partially because of some success in minimizing these gradients, the temperature measured at the center of the hotspot is often taken as a proxy of the temperature of the X-rayed sample (Boehler et al., 1990; Fiquet et al., 1996, 1998, 2000; Shen et al., 1998; Dewaele et al., 2000; Shim et al., 2000; Andrault and Fiquet, 2001; Kavner and Duffy, 2001). In all of these experiments, the central temperature is certainly an upper bound on the actual average temperature experienced by the sample volume that has a strong downward

bias due both axial and radial temperature gradients (Kavner et al., 1998).

In this paper we examine the sensitivity of thermoelastic properties (measured by combined laser heating and X-ray diffraction) to the temperature gradients. To help address this issue, we propose several alternative methods to measure the radial temperature gradients present in the laser-heated diamond anvil cell.

2. Effects on thermoelastic properties

Measurements of thermoelastic properties in the laser-heated diamond cell have exposed anomalous effects, such as lower than expected thermal expansion parameter for MgO (Fiquet et al., 1996) and/or unusually strong pressure-dependence of thermal expansion for both MgO (Fiquet et al., 1996) and iron (Boehler et al., 1990). These results have been ascribed to the presence of thermal pressure inside the diamond anvil cell, and may also arise from global pressure changes during the heating process. Table 1 shows that biases in temperature measurements due to the presence of a gradient can magnify the corresponding underestimate of thermal expansion determined by lattice parameters measured by X-ray diffraction. Measurements of well-calibrated internal standards in the hotspot show that the sample is generally found to follow a P - V path intermediate to constant volume and constant pressure conditions (Kavner and Duffy, 2001). In the case of constant volume, the thermal pressure is a maximum and thermal expansion is a minimum. In the case of constant pressure, the thermal expansion is a maximum and the thermal pressure is a minimum. In either case, assuming proper use of an internal standard, neglecting the influence of temperature gradients within the X-ray spot systematically underestimates the thermal expansion (Table 1).

The ratio of the half-width at half maximum (HWHM) of the X-ray beam to the hotspot HWHM spans a wide range depending on the experimental system, but should increase as pressure increases due to compression of the sample and insulation layer coupled with the high thermal conductivity of diamond (Bodea and Jeanloz, 1989; Kavner et al., 1998; Manga and Jeanloz, 1996; Panero and Jeanloz, 2001a,b). If this effect is not taken into account, the

Table 1

Calculations of thermoelastic properties for laser-heating experiments for a range of ratios of hotspot FWHM to the width of a square X-ray beam

T at X-ray beam edge (K)	Hotspot FWHM/size of X-ray beam (~square)	T , volume average (K)	Temperature underestimate (%)	Thermal expansion underestimate ^a (%)	Thermal pressure required to explain underestimate ^b (GPa)	Constant V : P_{thermal}	Thermal expansion underestimate (%)
2000	No temperature gradient across X-ray spot	2000	0	0	0	8.7	0
1900	0.95	1933	3.4	4	0.3	8.3	−3.9
1800	0.90	1865	6.8	8	0.7	8.0	−7.9
1500	0.75	1660	17	20	1.7	7.0	−19.5
1000	0.5	1312	34	40	3.5	5.2	−40.5

The average temperature of the X-rayed volume is calculated assuming a central hotspot temperature of 2000 K. Thermal expansion, α (in K^{-1}), is calculated the center temperature using as a proxy for the average temperature, and apparent thermal pressure (GPa) is calculated for the case of a material with $\alpha_0 = 30 \times 10^{-6}$ and $K_{0T} = 170$ GPa in the diamond anvil cell, ignoring the temperature gradient.

^a Assuming constant pressure.

^b Assuming sample chamber is intermediate between constant P and constant V .

apparent thermal expansion values show an anomalously steep decrease with pressure.

This is consistent with data from pioneering measurements on Fe (Boehler et al., 1990) and MgO (Fiquet et al., 1996) where the peak temperature was taken as a proxy for the sample temperature. In the case of iron, the results were interpreted as intrinsic thermoelastic properties of Fe (i.e. a steep decrease of thermal expansion with increasing pressure). In the past, thermal pressure has been invoked explain this (Heinz, 1990; Fiquet et al., 1996, 1998; Andrault et al., 1998; Dewaele et al., 1998). Thermal pressure, the pressure increase of a sample heated under constant volume conditions, is especially dependent on an accurate evaluation of the sample temperature because overestimating the average temperature of an X-rayed volume yields results that are indistinguishable from a thermal pressure. In order to differentiate the effects of thermal pressure and thermal expansion, special care must be taken to evaluate the temperature profile with respect to the volume of the X-rayed sample.

To calculate the average temperature of the X-rayed volume, the three-dimensional temperature profile must be integrated over the dimensions of the X-rayed spot. For a cylindrically symmetric laser-heated spot centered within the X-ray beam

$$T_{\text{avg}} = \frac{1}{XYt} \int_0^t \int_0^Y \int_0^X T(r, z) dx dy dz \quad (1)$$

where x and y describe the size and shape of the X-ray spot, t is the thickness of the sample, and $T(r, z)$ describes how the temperature profile varies across the X-ray volume, both radially (r) and axially (z). For a constant-intensity rectangular X-ray beam (X by Y), as would result from narrowing the beam using slits (Shen et al., 2001), no axial temperature gradients (double-sided laser heating in well-insulated opaque samples), and a radial Gaussian temperature profile with HWHM of σ

$$T_{\text{avg}} = (T_m - T_b) \pi \frac{\sigma^2}{XY} \text{erf} \left(\frac{X}{\sigma} \right) \text{erf} \left(\frac{Y}{\sigma} \right) + T_b \quad (2)$$

T_m is the peak (central) temperature and T_b the background temperature (300 K). As shown in Fig. 1 and Table 1, the average temperature of the X-ray volume is biased by the low temperatures at the perimeter of the X-ray spot. This bias will depend on the relative size and shape of both the X-ray beam profile and the temperature profile.

In practice, several factors conspire to complicate the volume integration of the complete temperature distribution $T(r, z)$ throughout an X-rayed sample. In addition to radial gradients, axial temperature gradients are always present in semi-transparent oxide and silicate samples (Manga and Jeanloz, 1996; Panero and Jeanloz, 2001a) and in samples that are heated from one side only in the case of more strongly absorbing samples. Such axial gradients will further reduce the

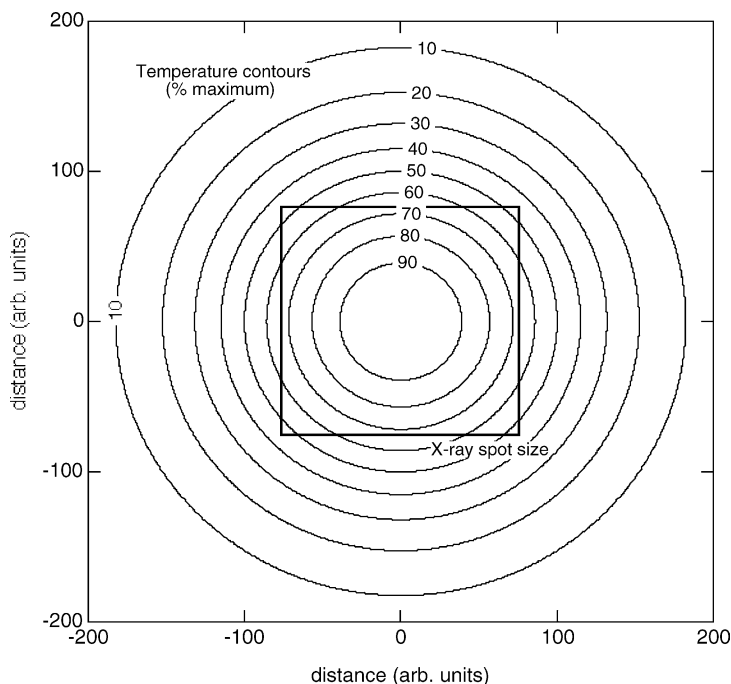


Fig. 1. Two-dimensional comparison of a Gaussian temperature profile with the size of a square X-ray beam.

average temperature of the X-rayed volume compared with the temperature measured in the center of the hotspot. In addition, the actual average temperature is very sensitive to the shape and intensity distribution of the X-ray beam and the spatial relationship between the laser beam and the X-ray beam. A square or rectangular X-ray beam will significantly lower the average temperature compared to the peak temperature because of the large volume contributed at the corners of the X-rayed sample, where temperature gradients may be significant; however, this effect is mitigated if X-ray intensity falls off towards the outer part of the X-ray beam. The exact shape and intensity profile of the X-ray beam must be accounted for in this integration.

Experimental results from double-sided heating of a platinum foil performed at GSECARS (Fig. 2) show representative temperature gradients relative to the size of the X-ray beam encountered during measurements of laser-heated Pt foil within the diamond cell. As pressure increases, the width of the hotspot decreases, as predicted by model calculations. The X-ray beam size for this experiment was $15\ \mu\text{m} \times 15\ \mu\text{m}$.

Therefore, at 12 GPa, the average temperature across the X-ray volume is 96% of the peak temperature. As pressure is increased to 20 GPa, the hotspot width decreases to $37\ \mu\text{m}$, and the average temperature drops to 93% of the temperature at the hotspot temperature.

These gradients are qualitatively similar to others reported in the literature. Temperature gradients for Fe are reported to be $\sim 15\ \text{K}/\mu\text{m}$, heated in conjunction with a $20\text{--}30\ \mu\text{m}$ diameter X-ray beam (Boehler et al., 1990). Assuming that the laser hotspot is perfectly centered within a rectangular-shaped X-ray beam, and that there are no axial temperature gradients, the average temperature under these conditions is 93–95% of the measured temperature at the hotspot center. Measurements on MgO were performed with an X-ray beam size of $50\ \mu\text{m} \times 50\ \mu\text{m}$ with a hotspot ranging from 75 to $100\ \mu\text{m}$ in diameter (Fiquet et al., 1996). Taking the diameter as the FWHM, and peak temperatures of 2000 K, the actual average temperature sampled by the X-ray beam ranges from 1585 K for a $75\ \mu\text{m}$ hotspot to 1747 K for a $100\ \mu\text{m}$ hotspot in these experiments, assuming a uniformly intense X-ray beam.

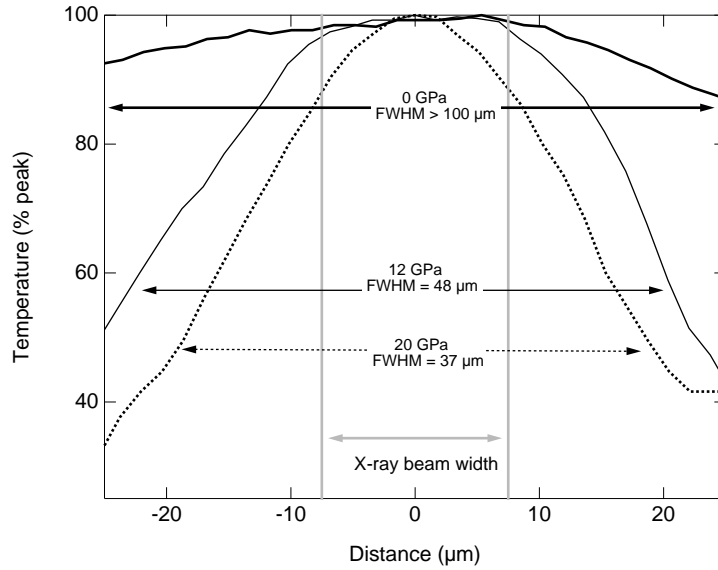


Fig. 2. Temperature measurements as a function of pressure for a platinum foil during double-sided laser heating with a Nd:YLF laser. The temperature was measured at each point of the hotspot image collected by a 100 μm entrance slit to an imaging spectrometer and CCD.

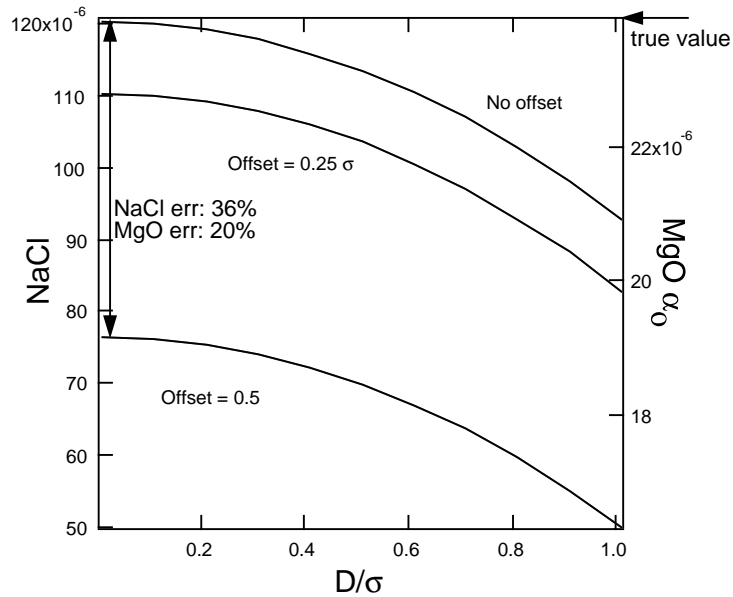


Fig. 3. Calculations of how misalignment between the X-ray and hotspot affects the thermal expansion measurement of NaCl and MgO assuming a Pt internal standard, 300 K pressure of 30 GPa, and peak temperature of 2000 K. The X-axis is a dimensionless measure of the size of the hotspot compared with the size of the X-ray beam. The X-ray beam is modeled as a square, with length D , and σ is the half-width at half maximum of the hotspot intensity. For the case of no offset, the curve shows the effect of not taking the temperature variations within the sample volume into account.

Because of the sensitive relationship between the center of the X-ray spot and the laser-heated spot, the most serious errors in thermoelastic properties may arise from small but systematic misalignments. For example, for a 30 μm -HWHM hotspot with the same width as the X-ray spot (D) a 2 μm misalignment causes the average temperature to decrease by $\sim 4\%$. For a typical system magnification of $12\times$, and CCD pixel size of 25 μm , a 2 μm misalignment is about 1 pixel in a measured temperature profile, and therefore not readily detectable in the data. Alignment becomes even more critical for measuring thermoelastic properties of materials. Fig. 3 shows explicitly the relationship between the X-ray spot and the hotspot, and how misalignment distorts measurements of thermal expansion. For example, to measure thermal expansions within 10%, the alignment must be within $1/4\sigma$ (where σ is the half-width at half-max of the hotspot intensity profile) or at GSECARS, better than 5 μm . Inaccurate measurements of the temperature gradient contribute a greater error. In contrast to random errors in temperature measurement, failure to account for the temperature gradients and misalignments in the experiment will lead to systematic errors. If the temperature system is properly aligned and calibrated, these systematic errors will always overestimate X-ray sampled temperatures, resulting in underestimates of thermal expansion parameters. Since pressure tends to steepen the temperature gradients, these effects become increasingly more significant with pressure. Therefore, a precise measurement of the temperature gradient is required to evaluate pressure-dependent thermoelastic properties. In the next section, we describe a new approach to measure temperatures and temperature gradients inside the laser-heated diamond cell.

3. Analysis of temperature measurement

The pioneering high-temperature measurements in the diamond anvil cell relied on optical pyrometry (Ming and Bassett, 1974) while almost all of the subsequent work has used spectral radiometry to measure temperature (Jeanloz and Heinz, 1984; Heinz and Jeanloz, 1987). In this section we delve into the spectroradiometric measurement, discussing a suite of techniques based on Planck's law to use the measured intensity data from a laser-heated spot in the diamond

anvil cell to calculate a central temperature and radial gradients. In addition to a direct fit of the spectral intensity to a graybody version of Planck's law, three additional techniques provide methods to evaluate the accuracy, precision and validity of a temperature measurement at high pressures within the diamond cell, and to make a precise estimate of the radial temperature gradient. For each method we present data from a hypothetical two-dimensional hotspot with a central temperature of 2500 K and a HWHM of 18 μm .

3.1. Peak temperature: full spectral fit to Planck's law

Temperature at each distance step across the hotspot is measured by fitting the calibrated and corrected spectral intensity (Schneider and Goebel, 1984) to Wien's approximation to Planck's law. Planck's law relates the spectral intensity ($I(\lambda)$), emissivity (ε), wavelength (λ) and temperature (T) of a blackbody-like thermal emitter through the relation:

$$I(\lambda, T) = 2\varepsilon(\lambda, T)\pi hc^2 \lambda^{-5} \left[\exp\left(\frac{hc}{\lambda kT}\right) - 1 \right]^{-1} \quad (3)$$

where c , k and h are the speed of light, Boltzmann's constant and Planck's constant, respectively.

Wien's approximation ($e^{hc/\lambda kT} \gg 1$) provides a linear relationship between spectral intensity and frequency, assuming constant emissivity (Jeanloz and Heinz, 1984; Heinz and Jeanloz, 1987). Temperature as a function of distance across the hotspot is calculated by fitting the spectral intensity to Wien's approximation of Planck's law, assuming a constant emissivity (ε) as a function of wavelength (λ) across the visible range:

$$I(\lambda, T) = 2\varepsilon\pi hc^2 \lambda^{-5} \left[\exp\left(\frac{-hc}{\lambda kT}\right) \right] \quad (4)$$

where the normalized intensity is defined as

$$J \sim \ln(I\lambda^5) \quad (5)$$

and the normalized frequency is

$$\omega = -\frac{hc}{\lambda k} \quad (6)$$

The linearized form of (4) allows temperature to be determined from the slope of normalized intensity

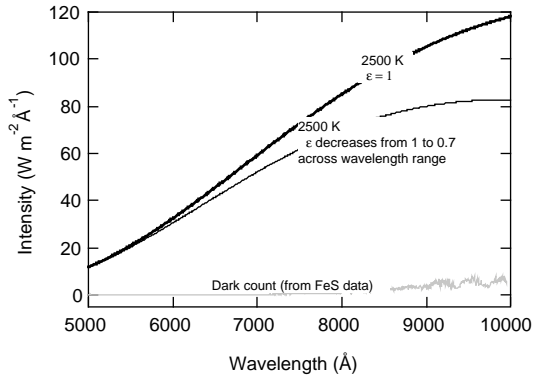


Fig. 4. Intensity as a function of wavelength for synthetic data set at 2500 K. Bold line shows spectral intensity for a blackbody. The thin black line shows calculated spectral intensity for a material whose emissivity decreases by 30% over the spectral range. The gray line shows experimental measurements obtained at GSECARS of dark noise on the CCD in an area away from an FeS hotspot.

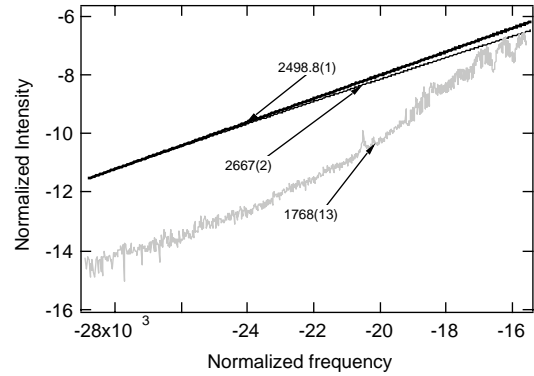


Fig. 5. Wien's plots of spectral data from the hotspot center. Normalized intensity (J) is plotted as a function of normalized frequency (see Eqs. (3) and (4) in text). Synthetic data set showing the Wien's plots are shown for the three cases in Fig. 4. Bold line: emissivity is constant; thin line: emissivity falls by 30%; gray line: Wien's plot of dark noise (once corrected for system response).

(Eq. (5)) plotted as a function of normalized frequency (Eq. (6)). The error introduced by using Wien's approximation to Planck's law is well understood, and ranges from less than 0.2% below 3500 K to less than 0.6% at 4500 K. A direct fit to Planck's law (assuming graybody behavior) is mathematically equivalent to fitting to the linearized Wien's law, because both methods fit only the same two adjustable parameters, T and ϵ , and the fitting errors are identical.

Linearity of the Wien plot is a necessary, but not sufficient, condition to assess the accuracy of a temperature measurement. The interdependence of the J and ω axes can hide serious errors such as those arising from chromatic aberration or diffraction effects within a linear-appearing Wien's plot. For example, a material with a 30% decrease in emissivity over the measured wavelength region (Fig. 4) will yield a temperature overestimate of 7%, or 165 K for a material emitting at 2500 K which is not resolved on the Wien plot, where the data appear linear (Fig. 5). To consider a worst-case example: even a spectrum of dark noise will generate a monotonically increasing function on a Wien plot (Fig. 5), and a straight-line fit through the data yields a temperature with an apparent precision of 0.7%. This is because the normalization technique magnifies the long wavelength intensity compared with the lower wavelength intensity. This is an inherent problem using this normalization technique, providing motivation

to (1) crosscheck the raw data and (2) explore additional and complementary techniques to measure temperature from spectral intensity data.

3.2. Peak temperature: two-color pyrometry

Two-color pyrometry is a complementary method to analyze temperature data that may underscore wavelength-dependent irregularities arising from either emissivity variations or optical misalignments and miscalibrations. Two-color pyrometry is based on the same intensity normalization scheme outlined in the previous section, except instead of calculating a single temperature from the complete spectral data set, a series of temperatures are calculated from pairs of intensities separated by a fixed spectral difference, $\omega_1 - \omega_2$:

$$T = \frac{\omega_2 - \omega_1}{J(\omega_2) - J(\omega_1)} \quad (7)$$

J and ω are defined in Eqs. (5) and (6). By scanning the spectral window across the measured spectral range, temperature can be determined as a function of wavelength, depending on the width of the spectral window. The wavelength interval needs to be small enough so that the temperature measurements are relatively unaffected by possible wavelength-dependent emissivity, but large enough so that the corresponding intensity differences are significant.

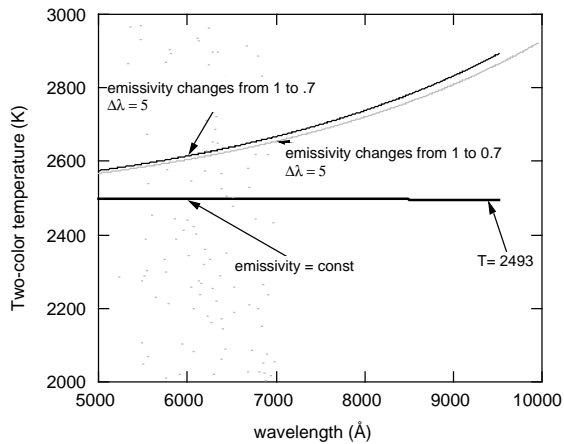


Fig. 6. Plots of two-color temperature as a function of wavelength for the spectral data shown in Fig. 4. The bold line shows the case for a graybody emitter. The thin lines show how temperature varies using a two-color pyrometer for the cases where emissivity decreases linearly across the spectral range, with the black line calculated using a window size of 500 Å, and the gray line using a window size of 50 Å.

In the ideal case, graybody radiation will yield a constant temperature across the wavelength range (Fig. 6). However, wavelength-dependent effects such as a slight miscalibration of the wavelength, optical misalignments, and wavelength-dependent emissivity will all introduce structure into a plot of temperature versus wavelength, some of which might bias the average slope on a Wien plot to higher or lower values, though not necessarily due to lower or higher temperatures. For example, the synthetic data showing a decrease in emissivity across the spectral range shows both an offset and an increasing temperature as a function of wavelength on the two-color plot (Fig. 6). For comparison, a tungsten filament decreases in emissivity only 10% over this range [http://www.pyrometry.com/relative_emissivity.html], yielding an even smaller effect than the example given in Fig. 6. Additionally, the dark noise data looks just like noise on the two-color plot. Thus, two-color pyrometry can be used to earmark meaningless data, and to help gauge the accuracy of temperatures determined by spectroradiometry by directly testing the graybody assumption. If the temperature is constant across the spectral range, the values can be accepted. Varying temperatures in the spectral range can indicate a problem—either wavelength-dependent emissivity

effects, or an alignment or calibration problem with a chromatic signature. The pyrometry plot also has the advantage in its sensitivity to thermally induced electronic excitations that fluoresce visible light. For example, luminescence from stressed pressure media such as NaCl that is superimposed on the Planck function will show up as extreme thermal deviations at specific wavelengths if a narrow band wavelength filter is chosen for the analysis.

Even in the best case, the data from two-color pyrometry may be noisy and difficult to interpret. Perhaps the complexity of the two-color pyrometry plots are the reason that even though this method has been previously noted (Heinz and Jeanloz, 1987) it is rarely employed. Temperature analysis by two-color pyrometry could be misleading if it were not used in conjunction with other temperature measurement techniques. It is problematic because it magnifies noise and other errors. Unlike a direct fit to Wien's approximation to Planck's law (Fig. 5), the results from two-color pyrometry are a sensitive indicator of errors arising from miscalibration of wavelength and system response. Therefore, the temperature variation across a two-color pyrometry plot is a more realistic assessment of the precision in the temperature measurement than the goodness of fit to Planck's law. The use of varying-sized windows and spectral neighborhood averaging may allow for more interpretable results from two-color pyrometry methods.

3.3. Temperature gradients: spectral intensity

The above two methods make a temperature measurement only at a single place on the hotspot, usually the center, where intensity is brightest, the gradient at a minimum, and is least contaminated by possible spectral effects from the optical system. The assumption that the central temperature is best-determined is implicit in most of the laser-heating experiments (Andraut and Fiquet, 2001; Shen et al., 2001; Watanuki et al., 2001; Yagi et al., 2001). Temperature gradient measurements using the spectroradiometry-based analysis usually require either scanning an aperture across the hotspot, which physically selects different areas of the hotspot (Boehler, 2000), or by employing a two-dimensional detector in conjunction with an imaging spectrometer that can measure temperature gradients in one

dimension (Kavner and Jeanloz, 1998b). The next two methods take advantage of the relationship between intensity and temperature described by Planck's law to use the central temperature as an anchor point to determine the radial temperature gradient. With these techniques an accurate measurement of the radial temperature gradient, relative to the central part of the hotspot, can be determined and the extent of chromatic aberrations can be quantitatively evaluated, as seen in the final section of the paper.

Assuming constant emissivity with temperature, Planck's law (Eq. (3)) yields a simple relative relationship between temperature and the intensity at a given wavelength:

$$\log \left(\frac{I_2(\lambda_0)}{I_{\max}(\lambda_0)} \right) \propto \frac{1}{T_{\max}} - \frac{1}{T_2} \quad (8)$$

I_{\max} and T_{\max} refer to the intensity and temperature, respectively, from the hotspot center. Since imaging spectroradiometry measures intensity as a function of wavelength and distance across the hotspot, this relationship can be used to calculate the temperature gradient, relative to the peak temperature, by using the peak temperature and intensity as an anchor point to scale the temperature with the intensity. Because of the strong dependence of intensity on temperature (a 50% change in intensity yields less than an 18% change in temperature), this technique generates an extremely precise measurement of the temperature gradient, relative to the central hotspot temperature. Using this technique, temperatures can be measured at much lower intensities than are allowable by spectroradiometry where the temperature calculation becomes extremely sensitive to both chromatic aberrations and dark noise at the hotspot edge, as shown in the last section of this paper.

Assuming counting statistics for uncertainties in the intensity measurements, the uncertainty in the temperatures measured through this technique are:

$$\frac{\delta T_2}{T_2} = \sqrt{\left(\frac{\delta T_m T_2}{T_m^2} \right)^2 + \left(\frac{\lambda k}{hc} \frac{T_2}{\sqrt{T_2}} \right)^2} \quad (9)$$

3.4. Temperature gradients: integrated intensity

The final method is similar to the previous method, but the sum of all of the measured intensities is used to calculate a temperature gradient instead of using

only a single wavelength. Integrating the differential form of Wien's approximation to Planck's law in the spectral range of interest yields:

$$\int_{\lambda_1}^{\lambda_2} I d\lambda = 2\epsilon\pi c^2 h \left(\frac{kT}{hc} \right)^4 (f(\lambda_2) - f(\lambda_1)) \quad (10)$$

$$f(\lambda) = \left(\left(\frac{m}{\lambda} \right)^3 + 3 \left(\frac{m}{\lambda} \right)^2 + 6 \left(\frac{m}{\lambda} \right) + 6 \right) e^{-m/\lambda} \quad (11)$$

where $m = hc/kT$. In the limit of $\lambda_1 = 0$ and $\lambda_2 = \infty$, this reduces to the Stephan-Boltzmann equation. The results are very similar to the previous method. Because summing the intensities across the spectral range increases the signal to noise ratio of the data, better temperature measurements towards the lower-temperature edges of the hotspot can be made with this technique. This process has virtually the same effect as averaging the results from the previous method.

4. Application to synthetic one-dimensional temperature measurement

To show how these last two analysis methods remove the potency of the chromatic aberration issue, we show here (1) how small amounts of chromatic aberration and optical misalignment can create a false belief of a "flat-top" hotspot, and (2) how the scaling methods outlined above can be applied to generate an improved, accurate measurement of the temperature profile.

Intensity as a function of distance and wavelength (4000–8950 Å) was calculated according to Planck's law for a Gaussian temperature profile (HWHM = 15 μm) with peak temperature, $T_{\max} = 3000$ K. We then model the effects of incorrect background subtraction, poor focusing and CCD rotation has on the resultant temperature measurement. Codes for the synthetic calculations can be found in the supplemental data. Fig. 7a shows the original temperature profile (thick solid line), plus temperature profiles generated via a Wien's law fit (thin solid line). Corresponding temperature-dependent, wavelength-independent apparent emissivity values are shown in Fig. 7b. To

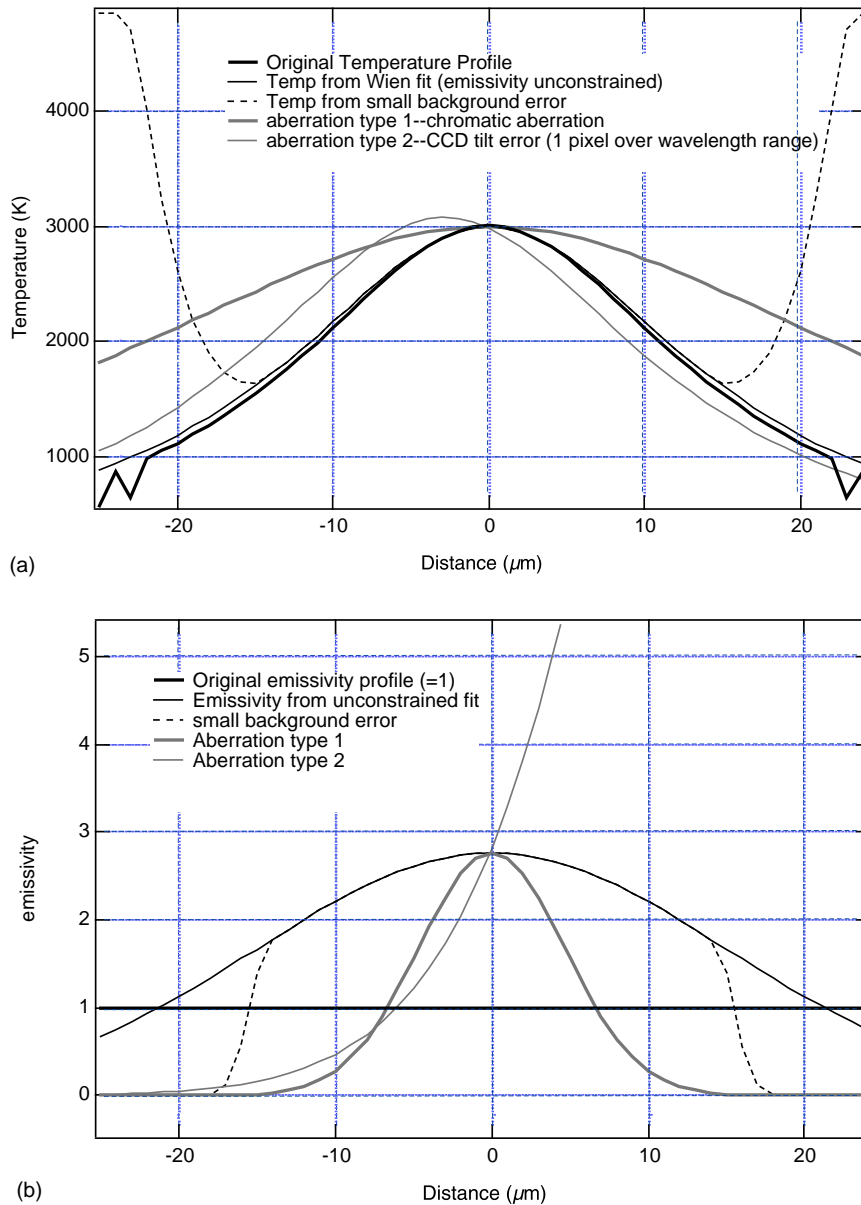


Fig. 7. Systematic errors in temperature measurements. (a) Modeled one-dimensional temperature profiles. The thick solid black line is the original temperature gradient, with a peak temperature of 3000 K and a half-width at half maximum of 15 μm . Thin black line: temperature as a function of distance recalculated using emissivity as a free parameter. Dashed line: Temperature calculated with an error in background correction (see text). Thick gray line: Temperature calculated using method 1 for a hotspot with chromatic aberration due to focusing. Thin gray line: Temperature calculated assuming a tilt error on a two-dimensional detector (see text). (b) Corresponding apparent temperature-dependent emissivities.

examine effects of small optical aberrations and misalignments on a synthetic hotspot measurement, the intensity profile at each distance was then recalculated with the wavelength-dependent Gaussian parameters adjusted to simulate measurement errors.

To simulate problems with incorrect background calibration, intensity values below a cutoff of 10 were automatically set to equal 10. Since the maximum intensities are $\sim 10^6$, this represents a 10 ppm error in background calibration. The effect on the inferred temperature is dramatic: with a temperature a non-monotonic function of distance, and showing an obviously non-physical result of temperature increasing with distance from the center of the hotspot (dashed line, Fig. 7a). Even at σ ($15 \mu\text{m}$), the temperature errors are significant, in excess of 400 K. Note the “wings” generated in the temperature profile; a feature sometimes observed in experimental measurements (e.g. *Jeanloz and Kavner, 1996*).

For an optical system that focuses red more tightly than blue, the effects are to give a significantly broader hotspot (thick gray line, Fig. 7a). We simulate this effect with a linear decrease in the intensity versus distance Gaussian width as a function of wavelength, with a Gaussian profile 16% wider at 4000 \AA and 11%

narrower at 8950 \AA than when focused. This extent of chromatic aberration is in line with alternate calculations (*Walter et al., this issue*). The effect is to produce a nearly flat temperature profile, with apparent temperatures 1000 K greater than the actual temperature at $15 \mu\text{m}$, alternately interpreted as a hotspot with a HWHM of $33 \mu\text{m}$.

A slight rotation of the CCD image plane with respect to the spectral distribution has yet another effect on the inferred temperature distribution. If the CCD is tilted such that the peak intensity at 4000 \AA hits the CCD just 1 pixel below where the peak intensity hits at 8950 \AA , this results in the peak intensities having slightly different centers across the wavelength range. This corresponds approximately to the alignment resolution capable in several existing temperature measurement systems. The effect on the inferred temperature distribution is a fair representation of the temperature gradient, but the peak temperature provides a $\sim 80 \text{ K}$ overestimate, and is off center from the actual peak by about $3 \mu\text{m}$. Referring to Fig. 3, if the laser position were “corrected” back to the center ($r = 0$), the now offset hotspot would give an underestimate of thermal expansions of 5% for MgO and 8% for NaCl.

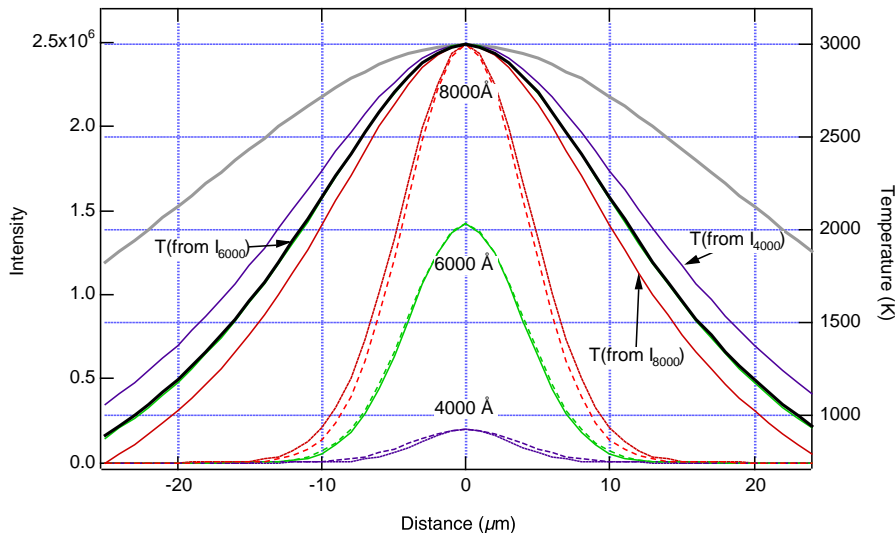


Fig. 8. Intensity profiles at 4000 , 6000 , and 8000 \AA (dotted lines, left axis) and corresponding temperature profiles (solid lines, right axis) plotted as a function of distance. The thick black line is the original temperature profile. The thick gray line is the same as thick gray line. The thin gray lines are temperatures recalculated by scaling intensities as a function of distance, using the central temperature and intensity as a reference point (see method 3 in text). The dotted lines are the original intensity vs. distance profiles for the synthetic hotspot. The dashed lines are the intensities after applying a focusing-chromatic aberration.

As shown in all three cases, moderate aberrations and misalignments can result in extremely misleading temperature profiles. There is some information in the apparent emissivity profiles; however, even the emissivity profile of the “best” temperature measurement (thin black line) does not appear significantly qualitatively different from what might be considered the worst case: a flatter apparent hotspot than the actual temperature distribution (thick gray line).

By scaling the temperature measurement to the spectral and integrated intensity profile, as in the last two methods outlined in the previous section, these aberrations can be examined and diagnosed. Fig. 8 shows intensity profiles at 4000, 6000, and 8000 Å; both the original intensity profile, and with the above proscribed chromatic aberrations due to the red end of the wavelength having a tighter focus than the blue end. These aberrations have a small effect on the intensity distribution (Fig. 8, dashed lines); however, the intensity information combines to create strong biases in the apparent temperature determined by fitting to spectral intensity to a blackbody curve (thick gray lines in Fig. 7a and 8). Overlaid on Fig. 8 is the original temperature distribution, and temperature distributions created by scaling the intensity profiles at each of the three wavelengths to the central temperature. At a distance of 10 μm from the center part of the spot, fitting the spectral intensity data to a blackbody curve generates large errors—in this case, 545 K. This error is bypassed when the intensities, even suffering from chromatic aberrations, are scaled with the temperature and corresponding intensity at the center of the hotspot: at 4000 Å, the temperature is overestimated by only 145 K. At 8000 Å, the temperature is underestimated by 150 K. In the middle of the spectral range, the temperature profile is reproduced exactly. Therefore, a consideration of how intensity scales with temperature will significantly improve the measurement of the temperature gradient. This information will help clarify and evaluate measurements of thermoelastic properties in the synchrotron-based laser-heated diamond anvil cell.

5. Conclusion

Taken together, these four techniques, along with an examination of the raw spectral intensity data,

provide a means to measure temperature, temperature gradients across a hotspot, and to realistically assess the accuracy and precision of those measurements. In the near future, the laser heating system that is currently under construction at UCLA will be employed to systematically test and evaluate these tests and corrections.

Acknowledgements

We thank Denis Andraut, Dion Heinz, Raymond Jeanloz, Mark Rivers, Guoyin Shen, and Dave Walker for comments and discussions. Portions of this work were performed at GeoSoilEnviroCARS (GSECARS), Sector 13, Advanced Photon Source at Argonne National Laboratory. GSECARS is supported by the National Science Foundation, Earth Sciences, Department of Energy, Geosciences, W.M. Keck Foundation and the United States Department of Agriculture. Use of the Advanced Photon Source was supported by the U.S. Department of Energy, Basic Energy Sciences, Office of Energy Research, under Contract No. W-31-109-Eng-38. AK acknowledges a Lamont-Doherty Earth Observatory postdoctoral fellowship and WRP acknowledges the Tuner postdoctoral fellowship from the University of Michigan for partial support of this work.

References

- Andraut, D., 2001. Evaluation of (Mg, Fe) partitioning between silicate perovskite and magnesiowüstite up to 120 GPa and 2300 K. *J. Geophys. Res.* 106, 2079–2087.
- Andraut, D., Fiquet, G., 2001. Synchrotron radiation and laser heating in a diamond anvil cell. *Rev. Sci. Instrum.* 72, 1283–1288.
- Andraut, D., Fiquet, G., Itie, J.P., Richet, P., Gillet, P., Hausermann, D., Hanfland, M., 1998. Thermal pressure in the laser-heated diamond-anvil cell: an X-ray diffraction study. *Eur. J. Mineral.* 10, 931–940.
- Bodea, S., Jeanloz, R., 1989. Model calculations of the temperature distribution in the laser-heated diamond cell. *J. Appl. Phys.* 65, 4688–4692.
- Boehler, R., 1992. Melting of the Fe–FeO and the Fe–FeS systems at high-pressure—constraints on core temperatures. *Earth Planet. Sci. Lett.* 111, 217–227.
- Boehler, R., 2000. High-pressure experiments and the phase diagram of lower mantle and core materials. *Rev. Geophys.* 38, 221–245.

- Boehler, R., Barga, N.V., Choplas, A., 1990. Melting, thermal expansion, and phase transition of iron at high pressures. *J. Geophys. Res.* 95, 21731–21736.
- Boehler, R., Chopelas, A., 1991. A new approach to laser-heating in high-pressure mineral physics. *Geophys. Res. Lett.* 18, 1147–1150.
- Boehler, R., Ross, M., 1997. Melting curve of aluminum in a diamond cell to 0.8 Mbar: implications for iron. *Earth Planet. Sci. Lett.* 153, 223–227.
- Boehler, R., Ross, M., Boeker, D.B., 1997. Melting of LiF and NaCl to 1 Mbar: systematics of ionic solids at extreme conditions. *Phys. Rev. Lett.* 78, 4589–4592.
- Dewaele, A., Fiquet, G., Andrault, D., Hausermann, D., 2000. P - V - T equation of state of periclase from synchrotron radiation measurements. *J. Geophys. Res.* 105, 2869–2877.
- Dewaele, A., Fiquet, G., Gillet, P., 1998. Temperature and pressure distribution in the laser-heated diamond-anvil cell. *Rev. Sci. Instrum.* 69, 2421–2426.
- Fiquet, G., Andrault, D., Dewaele, A., Charpin, T., Kunz, M., Hausermann, D., 1998. P - V - T equation of state of MgSiO_3 perovskite. *Phys. Earth Planet. Inter.* 105, 21–31.
- Fiquet, G., Andrault, D., Itie, J.P., Gillet, P., Richet, P., 1996. X-ray diffraction of periclase in a laser-heated diamond-anvil cell. *Phys. Earth Planet. Inter.* 95, 1–17.
- Fiquet, G., Dewaele, A., Andrault, D., Kunz, M., Le Bihan, T., 2000. Thermoelastic properties and crystal structure of MgSiO_3 perovskite at lower mantle pressure and temperature conditions. *Geophys. Res. Lett.* 27, 21–24.
- Heinz, D.L., 1990. Thermal pressure in the laser-heated diamond anvil cell. *Geophys. Res. Lett.* 17, 1161–1164.
- Heinz, D.L., Jeanloz, R., 1987. Temperature measurements in the laser-heated diamond anvil cell. In: Manghnani, M., Syono, Y. (Eds.), *High-pressure Research in Mineral Physics*. American Geophysical Union, Washington, DC, pp. 113–127.
- Jeanloz, R., Heinz, D.L., 1984. Experiments at high temperature and pressure-laser heating through the diamond cell. *J. Phys. (Paris)* 45, 83–92.
- Jeanloz, R., Kavner, A., 1996. Melting criteria and imaging spectroradiometry in laser-heated diamond-cell experiments. *Phil. Trans. R. Soc. Lond., Ser. A: Math. Phys. Eng. Sci.* 354, 1279–1305.
- Kavner, A., Duffy, T.S., 2001. Pressure–volume–temperature paths in the laser-heated diamond anvil cell. *J. Appl. Phys.* 89, 1907–1914.
- Kavner, A., Duffy, T.S., Heinz, D., Shen, G., 1998. Thermoelastic behavior of platinum and MgO in the laser-heated diamond anvil cell. *Trans. Am. Geophys. U.* 79, S163.
- Kavner, A., Duffy, T.S., Shen, G.Y., 2001. Phase stability and density of FeS at high pressures and temperatures: implications for the interior structure of Mars. *Earth Planet. Sci. Lett.* 185, 25–33.
- Kavner, A., Jeanloz, R., 1998a. The high-pressure melting curve of Allende meteorite. *Geophys. Res. Lett.* 25, 4161–4164.
- Kavner, A., Jeanloz, R., 1998b. High-pressure melting curve of platinum. *J. Appl. Phys.* 83, 7553–7559.
- Lazor, P., Shen, G., Saxena, S.K., 1993. Laser-heated diamond-anvil cell experiments at high-pressure-melting curve of nickel up to 700 Kbar. *Phys. Chem. Miner.* 20, 86–90.
- Li, X.Y., Manga, M., Nguyen, J.H., Jeanloz, R., 1996. Temperature distribution in the laser-heated diamond cell with external heating, and implications for the thermal conductivity of perovskite. *Geophys. Res. Lett.* 23, 3775–3778.
- Manga, M., Jeanloz, R., 1996. Axial temperature gradients in dielectric samples in the laser-heated diamond cell. *Geophys. Res. Lett.* 23, 1845–1848.
- Ming, L.C., Bassett, W.A., 1974. Laser heating in the diamond anvil press up to 2000C sustained and 3000C pulsed. *Rev. Sci. Instrum.* 45, 1115–1118.
- Panero, W.R., Jeanloz, R., 2001a. Temperature gradients in the diamond anvil cell. *J. Geophys. Res.* 106, 6493–6498.
- Panero, W.R., Jeanloz, R., 2001b. The effect of sample thickness and insulation layers on the temperature distribution in the laser-heated diamond cell. *Rev. Sci. Instrum.* 72, 1306–1308.
- Saxena, S.K., Shen, G., Lazor, P., 1994. Temperatures in Earth's core based on melting and phase-transformation experiments on iron. *Science* 264, 405–407.
- Schneider, W.E., Goebel, D.G., 1984. Technical note. *Laser Focus/Electro-Optics* 20, 90.
- Shen, G.Y., Mao, H.K., Hemley, R.J., Duffy, T.S., Rivers, M.L., 1998. Melting and crystal structure of iron at high pressures and temperatures. *Geophys. Res. Lett.* 25, 373–376.
- Shen, G.Y., Rivers, M.L., Wang, Y.B., Sutton, S.R., 2001. Laser heated diamond cell system at the advanced photon source for in situ X-ray measurements at high pressure and temperature. *Rev. Sci. Instrum.* 72, 1273–1282.
- Shim, S.H., Duffy, T.S., Shen, G.Y., 2000. The stability and P - V - T equation of state of CaSiO_3 perovskite in the Earth's lower mantle. *J. Geophys. Res.* 105, 25955–25968.
- Shim, S.H., Duffy, T.S., Shen, G.Y., 2001. The post-spinel transformation in Mg_2SiO_4 and its relation to the 660-km seismic discontinuity. *Nature* 411, 571–574.
- Sitaud, B., Thevenin, T., 1999. Melting-point measurements at high static pressures from laser heating methods: application to uranium. *Int. J. Thermophys.* 20, 1189–1198.
- Sweeney, J.S., Heinz, D.L., 1993. Thermal-analysis in the laser-heated diamond-anvil cell. *Pure Appl. Geophys.* 141, 497–507.
- Watanuki, T., Shimomura, O., Yagi, T., Kondo, T., Isshiki, M., 2001. Construction of laser-heated diamond anvil cell system for in situ X-ray diffraction study at SPring-8. *Rev. Sci. Instrum.* 72, 1289–1292.
- Williams, Q., Jeanloz, R., 1990. Melting relations in the iron–sulfur system at ultra-high pressures—implications for the thermal state of the Earth. *J. Geophys. Res.* 95, 19299–19310.
- Williams, Q., Knittle, E., Jeanloz, R., 1991. The high-pressure melting curve of iron—a technical discussion. *J. Geophys. Res.* 96, 2171–2184.
- Yagi, T., Kondo, T., Watanuki, T., Shimomura, O., Kikegawa, T., 2001. Laser heated diamond anvil apparatus at the Photon Factory and SPring-8: problems and improvements. *Rev. Sci. Instrum.* 72, 1293–1297.
- Yoo, C.S., Akella, J., Moriarty, J.A., 1993. High-pressure melting temperatures of uranium—laser-heating experiments and theoretical calculations. *Phys. Rev. B* 48, 15529–15534.